# HARBOR RESONANCES IN COASTAL ENGINEERING

## 6.1 Introduction

In this chapter we consider the application of the half-plane Helmholtz problem described in Chapter III to the computation of harbor resonances in coastal engineering.

We consider the problem of computing resonances for the Helmholtz equation in a two-dimensional compactly perturbed half-plane with an impedance boundary condition. One of its main applications corresponds to coastal engineering, acting as a simple model to determine the resonant states of a maritime harbor. In this model the sea is modeled as an infinite half-plane, which is locally perturbed by the presence of the harbor, and the coast is represented by means of an impedance boundary condition. Some references on the harbor oscillations that are responsible for these resonances are Mei (1983), Mei et al. (2005), Herbich (1999), and Panchang & Demirbilek (2001).

Resonances are closely related to the phenomena of seiching (in lakes and harbors) and sloshing (in coffee cups and storage tanks), which correspond to standing waves in enclosed or partially enclosed bodies of water. These phenomena have been observed already since very early times. Scientific studies date from Merian (1828) and Poisson (1828–1829), and especially from the observations in the Lake of Geneva by Forel (1895), which began in 1869. A thorough and historical review of the seiching phenomenon in harbors and further references can be found in Miles (1974).

Oscillations in harbors, though, were first studied for circular and rectangular closed basins by Lamb (1916). More practical approaches for the same kind of basins, but now connected to the open sea through a narrow mouth, were then implemented respectively by McNown (1952) and Kravtchenko & McNown (1955).

But it was the paper of Miles & Munk (1961), the first to treat harbor oscillations by a scattering theory, which really arose the research interest on the subject. Their work, together with the contributions of Le Méhauté (1961), Ippen & Goda (1963), Raichlen & Ippen (1965), and Raichlen (1966), made the description of harbor oscillations to become fairly close to the experimentally observed one. Theories to deal with arbitrary harbor configurations were available after Hwang & Tuck (1970) and Lee (1969, 1971), who worked with boundary integral equation methods to calculate the oscillation in harbors of constant depth with arbitrary shape. Mei & Chen (1975) developed a hybrid-boundary-element technique to also study harbors of arbitrary geometry. Harbor resonances using the finite element method are likewise computed in Walker & Brebbia (1978). A comprehensive list of references can be found in Yu & Chwang (1994).

The mild-slope equation, which describes the combined effects of refraction and diffraction of linear water waves, was first suggested by Eckart (1952) and later rederived by Berkhoff (1972*a*,*b*, 1976), Smith & Sprinks (1975), and others, and is now well-accepted as the method for estimating coastal wave conditions. It corresponds to an approximate model developed in the framework of the linear water-wave theory (vid. Section A.10), which assumes waves of small amplitude and a mild slope on the bottom of the sea, i.e., a slowly

varying bathymetry. The mild-slope equation models the propagation and transformation of water waves, as they travel through waters of varying depth and interact with lateral boundaries such as cliffs, beaches, seawalls, and breakwaters. As a result, it describes the variations in wave amplitude, or equivalently wave height. From the wave amplitude, the amplitude of the flow velocity oscillations underneath the water surface can also be computed. These quantities, wave amplitude and flow-velocity amplitude, may subsequently be used to determine the wave effects on coastal and offshore structures, ships and other floating objects, sediment transport and resulting geomorphology changes of the sea bed and coastline, mean flow fields and mass transfer of dissolved and floating materials. Most often, the mild-slope equation is solved by computers using methods from numerical analysis. The mild-slope equation is a usually expressed in an elliptic form, and it turns into the Helmholtz equation for uniform water depths. Different kinds of mild-slope equations have been derived (Liu & Shi 2008). A detailed survey of the literature on the mild-slope and its related equations is provided by Hsu, Lin, Wen & Ou (2006). Some examinations on the validity of the theory are performed by Booij (1983) and Ehrenmark & Williams (2001).

A resonance of a different type is given by the so-called Helmholtz mode when the oscillatory motion inside the harbor is much slower than each of the normal modes (Burrows 1985). It corresponds to the resonant mode with the longest period, where the water appears to move up and down unison throughout the harbor, which seems to have been first studied by Miles & Munk (1961) and which appears to be particularly significant for harbors responding to the energy of a tsunami. We remark that from the mathematical point of view, resonances correspond to poles of the scattering and radiation potentials when they are extended to the complex frequency domain (cf. Poisson & Joly 1991). Harbor resonance should be avoided or minimized in harbor planning and operation to reduce adverse effects such as hazardous navigation and mooring of vessels, deterioration of structures, and sediment deposition or erosion within the harbor.

Along rigid, impermeable vertical walls a Neumann boundary condition is used, since there is no flow normal to the surface. However, in general an impedance boundary condition is used along coastlines or permeable structures, to account for a partial reflection of the flow on the boundary (Demirbilek & Panchang 1998). A study of harbor resonances using an approximated Dirichlet-to-Neumann operator and a model based on the Helmholtz equation with an impedance boundary condition on the coast was done by Quaas (2003). In the current chapter this problem is extended to be solved with integral equation techniques, by profiting from the knowledge of the Green's function developed in Chapter III.

This chapter is structured in $4$ sections, including this introduction. The harbor scattering problem is presented in Section 6.2. Section 6.3 describes the computation of resonances for the harbor scattering problem by using integral equation techniques and the boundary element method. Finally, in Section 6.4 a benchmark problem based on a rectangular harbor is presented and solved numerically.

## 6.2 Harbor scattering problem

We are interested in computing the resonances of a maritime harbor, as the one depicted in Figure 6.1 The sea is modeled as the compactly perturbed half-plane $\Omega_e \subset \mathbb{R}^2_+$, where $\mathbb{R}^2_+ = \{(x_1, x_2) \in \mathbb{R}^2 : x_2 > 0\}$ and where the perturbation represents the presence of the harbor. We denote its boundary by $\Gamma$, which is regular (e.g., of class $C^2$) and decomposed according to $\Gamma = \Gamma_p \cup \Gamma_\infty$. The perturbed boundary describing the harbor is denoted by $\Gamma_p$, while $\Gamma_\infty$ denotes the remaining unperturbed boundary of $\mathbb{R}^2_+$, which represents the coast and extends towards infinity on both sides. The unit normal $\boldsymbol{n}$ is taken outwardly oriented of $\Omega_e$ and the land is represented by the complementary domain $\Omega_c = \mathbb{R}^2 \setminus \overline{\Omega_e}$.

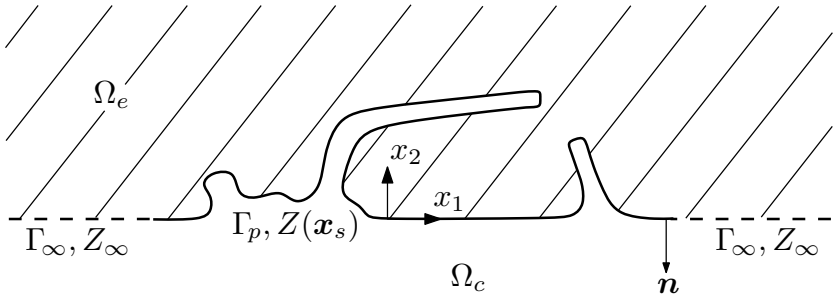


FIGURE 6.1. Harbor domain.

To describe the propagation of time-harmonic linear water waves over a slowly varying bathymetry we consider for the wave amplitude or surface elevation $\eta$ the mild-slope equation (Herbich 1999)

$$\operatorname{div}(cc_g\nabla\eta) + k^2 cc_g\eta = 0 \qquad \text{in } \Omega_e, \tag{6.1}$$

where $k$ is the wave number, where $c$ and $c_g$ denote respectively the local phase and group velocities of a plane progressive wave of angular frequency $\omega$, and where the time convention $e^{-i\omega t}$ is used. The local phase and group velocities are given respectively by

$$c = \frac{\omega}{k} \qquad \text{and} \qquad c_g = \frac{\mathrm{d}\omega}{\mathrm{d}k} = \frac{c}{2}\left(1 + \frac{2kh}{\sinh(2kh)}\right), \tag{6.2}$$

where $h$ denotes the local water depth. The wave number $k$ and the local depth $h$ vary slowly in the horizontal directions $x_1$ and $x_2$ according to the frequency dispersion relation

$$\omega^2 = gk\tanh(kh), \tag{6.3}$$

where $g$ is the gravitational acceleration. We remark that the mild-slope equation (6.1) holds also for the velocity potential $\phi$, since it is related to the wave height $\eta$ through

$$g\eta = i\omega\phi. \tag{6.4}$$

We observe furthermore that through the transformation $\psi = \sqrt{cc_g}\,\eta$, the mild-slope equation (6.1) can be cast in the form of a Helmholtz equation, i.e.,

$$\Delta\psi + k_c^2\psi = 0, \qquad \text{where } k_c^2 = k^2 - \frac{\Delta(cc_g)^{1/2}}{(cc_g)^{1/2}}. \tag{6.5}$$

In shallow water, when $kh \ll 1$, the difference $k_c^2 - k^2$ may become appreciable. In this case $\tanh(kh) \approx kh$ and $\sinh(kh) \approx kh$, and thus we have from (6.3) that (Radder 1979)

$$k^2 \approx \frac{\omega^2}{gh}, \qquad c \approx c_g \approx \sqrt{gh}, \qquad \text{and} \qquad k_c^2 \approx \frac{\omega^2}{gh} - \frac{\Delta h}{2h} + \frac{|\nabla h|^2}{4h^2}. \tag{6.6}$$

It follows that $k_c$ may be approximated by $k$ if

$$|\Delta h| \ll 2\omega^2/g \qquad \text{and} \qquad |\nabla h|^2 \ll 4\omega^2 h/g, \tag{6.7}$$

implying a slowly varying depth and a small bottom slope, or high-frequency wave propagation. Hence, if (6.7) is satisfied for shallow water, then we can readily work with the Helmholtz equation

$$\Delta\psi + k^2\psi = 0 \qquad \text{in } \Omega_e. \tag{6.8}$$

On the other hand, for short waves in deep water, when $kh \gg 1$, we have that $c_g \approx c/2$ is more or less constant and thus again the Helmholtz equation (6.8) applies. We observe that the Helmholtz equation holds as well whenever the depth $h$ is constant, i.e.,

$$\Delta\eta + k^2\eta = 0 \qquad \text{in } \Omega_e. \tag{6.9}$$

On coastline and surface-protruding structures, the following impedance or partial reflection boundary condition is used (cf., e.g., Berkhoff 1976, Tsay et al. 1989):

$$-\frac{\partial\eta}{\partial n} + Z\eta = 0 \qquad \text{on } \Gamma, \tag{6.10}$$

where the impedance $Z$ is taken as purely imaginary and typically represented by means of a reflection coefficient $K_r$ as (Herbich 1999)

$$Z = ik\,\frac{1 - K_r}{1 + K_r}. \tag{6.11}$$

The coefficient $K_r$ varies between 0 and 1, and specific values for different types of reflecting surfaces have been compiled by Thompson, Chen & Hadley (1996). Values of $K_r$ are normally chosen based on the boundary material and shape, e.g., for a natural beach $0.05 \le K_r \le 0.2$ and for a vertical wall with the crown above the water $0.7 \le K_r \le 1.0$. Effects such as slope, permeability, relative depth, wave period, breaking, and overtopping can be considered in selecting values within these fairly wide ranges. We note that $Z$ is equal to zero for fully reflective boundaries ($K_r = 1$) and it is equal to $ik$ for fully absorbing boundaries ($K_r = 0$). Thus the reflection characteristics of boundaries that are not fully reflective will inherently have some dependence on local wavelength through $k$. In practice, wave periods range from about 6 s to 20 s. For a representative water depth of 10 m, the value of $k$ ranges from 0.03 $\text{m}^{-1}$ to 0.13 $\text{m}^{-1}$. For long waves, $k$ and $Z$ become small, and boundaries may behave as nearly full reflectors regardless of the value of $K_r$. It may be verified that (6.10) is strictly valid only for fully reflecting boundaries ($K_r = 1$). For

partially reflecting boundaries, it is valid only if waves approach the boundary normally. For other conditions (6.10) is approximate and may produce distortions. More accurate boundary conditions are described in Panchang & Demirbilek (2001). In our model, we assume that the impedance can be decomposed as

$$Z(\boldsymbol{x}) = Z_\infty + Z_p(\boldsymbol{x}), \qquad \boldsymbol{x} \in \Gamma, \tag{6.12}$$

being $Z_\infty$ constant throughout $\Gamma$, and depending $Z_p(\boldsymbol{x})$ on the position $\boldsymbol{x}$ with a bounded support contained in $\Gamma_p$.

We consider now the direct scattering problem of linear water waves around a harbor. The total field $\eta$ is decomposed as $\eta = u_I + u_R + u$, where $u_I$ and $u_R$ are respectively the known incident and reflected fields, and where $u$ denotes the unknown scattered field. The goal is to find $u$ as a solution to the Helmholtz equation in $\Omega_e$, satisfying an outgoing radiation condition, and such that the total field $\eta$ satisfies a homogeneous impedance boundary condition on $\Gamma$. We have thus for the scattered field that

$$-\frac{\partial u}{\partial n} + Zu = f_z \qquad \text{on } \Gamma, \tag{6.13}$$

where $f_z$ is known, has its support contained in $\Gamma_p$, and is given by

$$f_z = \frac{\partial u_I}{\partial n} - Zu_I + \frac{\partial u_R}{\partial n} - Zu_R \qquad \text{on } \Gamma. \tag{6.14}$$

As $u_I$ we take an incident plane volume wave of the form (3.16), with a wave propagation vector $\boldsymbol{k} \in \mathbb{R}^2$ such that $k_2 \leq 0$. The reflected field $u_R$ is thus of the form (3.17) and has a wave propagation vector $\bar{\boldsymbol{k}} = (k_1, -k_2)$. Hence,

$$u_I(\boldsymbol{x}) = e^{i\boldsymbol{k}\cdot\boldsymbol{x}} \qquad \text{and} \qquad u_R(\boldsymbol{x}) = -\left(\frac{Z_\infty + ik_2}{Z_\infty - ik_2}\right) e^{i\bar{\boldsymbol{k}}\cdot\boldsymbol{x}}. \tag{6.15}$$

To eliminate the non-physical solutions, we have to impose also an outgoing radiation condition in the form of (3.6) for the scattered field $u$, i.e., when $r \to \infty$ it is required that

$$\begin{cases} |u| \leq \dfrac{C}{\sqrt{r}} \quad \text{and} \quad \left|\dfrac{\partial u}{\partial r} - iku\right| \leq \dfrac{C}{r} \quad \text{if } x_2 > \dfrac{1}{2Z_\infty}\ln(1+\beta r), \\ |u| \leq C \quad \text{and} \quad \left|\dfrac{\partial u}{\partial r} - i\xi_p u\right| \leq \dfrac{C}{r} \quad \text{if } x_2 \leq \dfrac{1}{2Z_\infty}\ln(1+\beta r), \end{cases} \tag{6.16}$$

for some constants $C > 0$, where $r = |\boldsymbol{x}|$, $\beta = 8\pi k Z_\infty^2/\xi_p^2$, and $\xi_p = \sqrt{Z_\infty^2 + k^2}$. The harbor scattering problem is thus given by

$$\begin{cases} \text{Find } u : \Omega_e \to \mathbb{C} \text{ such that} \\ \Delta u + k^2 u = 0 \qquad \text{in } \Omega_e, \\ -\dfrac{\partial u}{\partial n} + Zu = f_z \qquad \text{on } \Gamma, \\ \text{+ Outgoing radiation condition as } |\boldsymbol{x}| \to \infty, \end{cases} \tag{6.17}$$

where the outgoing radiation condition is stated in (6.16).

The problem of finding harbor resonances amounts to search wave numbers $k$ for which the scattering problem (6.17) without excitation, i.e., with $f_z = 0$, admits non-zero solutions $u$. The harbor resonance problem can be hence stated as

$$\begin{cases} \text{Find } k \in \mathbb{C} \text{ and } u : \Omega_e \to \mathbb{C},\ u \neq 0, \text{ such that} \\ \Delta u + k^2 u = 0 \qquad \text{in } \ \Omega_e, \\ -\dfrac{\partial u}{\partial n} + Zu = 0 \qquad \text{on } \ \Gamma, \\ \text{+ Outgoing radiation condition as } |\boldsymbol{x}| \to \infty. \end{cases} \tag{6.18}$$

## 6.3 Computation of resonances

The resonance problem (6.18) is solved in the same manner as the half-plane impedance Helmholtz problem described in Chapter III, by using integral equation techniques and the boundary element method. The required Green's function $G$ is expressed in (3.93). If we denote the trace of the solution on $\Gamma_p$ by $\mu = u|_{\Gamma_p}$, then we have from (3.156) that the solution $u$ admits the integral representation

$$u = \mathcal{D}(\mu) - \mathcal{S}(Z\mu) \qquad \text{in } \ \Omega_e, \tag{6.19}$$

where we define for $\boldsymbol{x} \in \Omega_e$ the single and double layer potentials respectively by

$$\mathcal{S}\nu(\boldsymbol{x}) = \int_{\Gamma_p} G(\boldsymbol{x}, \boldsymbol{y})\nu(\boldsymbol{y})\, \mathrm{d}\gamma(\boldsymbol{y}) \quad \text{and} \quad \mathcal{D}\mu(\boldsymbol{x}) = \int_{\Gamma_p} \frac{\partial G}{\partial n_{\boldsymbol{y}}}(\boldsymbol{x}, \boldsymbol{y})\mu(\boldsymbol{y})\, \mathrm{d}\gamma(\boldsymbol{y}). \tag{6.20}$$

If the boundary is decomposed as $\Gamma = \Gamma_0 \cup \Gamma_+$, being

$$\Gamma_0 = \{\boldsymbol{y} \in \Gamma :\ y_2 = 0\} \qquad \text{and} \qquad \Gamma_+ = \{\boldsymbol{y} \in \Gamma :\ y_2 > 0\}, \tag{6.21}$$

then $u$ admits also, from (3.163) and (3.164), the boundary integral representation

$$\frac{u}{2} = D(\mu) - S(Z\mu) \qquad \text{on } \ \Gamma_+, \tag{6.22}$$

$$u = D(\mu) - S(Z\mu) \qquad \text{on } \ \Gamma_0, \tag{6.23}$$

where the boundary integral operators, for $\boldsymbol{x} \in \Gamma$, are defined by

$$S\nu(\boldsymbol{x}) = \int_{\Gamma_p} G(\boldsymbol{x}, \boldsymbol{y})\nu(\boldsymbol{y})\, \mathrm{d}\gamma(\boldsymbol{y}) \quad \text{and} \quad D\mu(\boldsymbol{x}) = \int_{\Gamma_p} \frac{\partial G}{\partial n_{\boldsymbol{y}}}(\boldsymbol{x}, \boldsymbol{y})\mu(\boldsymbol{y})\, \mathrm{d}\gamma(\boldsymbol{y}). \tag{6.24}$$

It holds that (6.22) and (6.23) can be combined on $\Gamma_p$ into the single integral equation

$$(1 + \mathcal{I}_0)\frac{\mu}{2} + S(Z\mu) - D(\mu) = 0 \qquad \text{on } \ \Gamma_p, \tag{6.25}$$

where $\mathcal{I}_0$ denotes the characteristic or indicator function of the set $\Gamma_0$, i.e.,

$$\mathcal{I}_0(\boldsymbol{x}) = \begin{cases} 1 & \text{if } \ \boldsymbol{x} \in \Gamma_0, \\ 0 & \text{if } \ \boldsymbol{x} \notin \Gamma_0. \end{cases} \tag{6.26}$$

The desired resonances are thus given by the wave numbers $k$ for which the integral equation (6.25) admits non-zero solutions $\mu$. Care has to be taken, though, with possible spurious resonances that may appear for the integral equation, which are not resonances of

the original problem (6.18) and which are related with a resonance problem in the complementary domain $\Omega_c$. To find the resonances, we use the boundary element method on the variational formulation of (6.25). This variational formulation, as indicated in (3.198), searches $k \in \mathbb{C}$ and $\mu \in H^{1/2}(\Gamma_p)$, $\mu \neq 0$, such that $\forall \varphi \in H^{1/2}(\Gamma_p)$ we have that

$$\left\langle (1+\mathcal{I}_0)\frac{\mu}{2} + S(Z\mu) - D(\mu), \varphi \right\rangle = 0. \tag{6.27}$$

As performed in Section 3.11 and with the same notation, we discretize (6.27) employing a Galerkin scheme. We use on the boundary curve $\Gamma_p$ Lagrange finite elements of type $\mathbb{P}_1$. The curve $\Gamma_p$ is approximated by the discretized curve $\Gamma_p^h$, composed by $I$ rectilinear segments $T_j$, sequentially ordered from left to right for $1 \leq j \leq I$, such that their length $|T_j|$ is less or equal than $h$, and with their endpoints on top of $\Gamma_p$. The function space $H^{1/2}(\Gamma_p)$ is approximated using the conformal space of continuous piecewise linear polynomials with complex coefficients

$$Q_h = \big\{ \varphi_h \in C^0(\Gamma_p^h) \,:\, \varphi_h|_{T_j} \in \mathbb{P}_1(\mathbb{C}), \;\; 1 \leq j \leq I \big\}. \tag{6.28}$$

The space $Q_h$ has a finite dimension $(I+1)$, and we describe it using the standard base functions for finite elements of type $\mathbb{P}_1$, denoted by $\{\chi_j\}_{j=1}^{I+1}$. We approximate the solution $\mu \in H^{1/2}(\Gamma_p)$ by $\mu_h \in Q_h$, being

$$\mu_h(\boldsymbol{x}) = \sum_{j=1}^{I+1} \mu_j \, \chi_j(\boldsymbol{x}) \qquad \text{for } \; \boldsymbol{x} \in \Gamma_p^h, \tag{6.29}$$

where $\mu_j \in \mathbb{C}$ for $1 \leq j \leq I+1$. We characterize all the discrete approximations by the index $h$, including also the wave number, the impedance and the boundary layer potentials. The numerical approximation of (6.27) becomes searching $\mu_h \in Q_h$ such that $\forall \varphi_h \in Q_h$

$$\left\langle (1+\mathcal{I}_0^h)\frac{\mu_h}{2} + S_h(Z_h\mu_h) - D_h(\mu_h), \varphi_h \right\rangle = 0. \tag{6.30}$$

Considering this decomposition of $\mu_h$ in terms of the base $\{\chi_j\}$ and taking as test functions the same base functions, $\varphi_h = \chi_i$ for $1 \leq i \leq I+1$, yields the discrete linear system

$$\sum_{j=1}^{I+1} \mu_j \left( \frac{1}{2}\big\langle (1+\mathcal{I}_0^h)\chi_j, \chi_i \big\rangle + \langle S_h(Z_h\chi_j), \chi_i \rangle - \langle D_h(\chi_j), \chi_i \rangle \right) = 0. \tag{6.31}$$

This can be expressed as the linear matrix system

$$\begin{cases} \text{Find } k_h \in \mathbb{C} \text{ and } \boldsymbol{\mu} \in \mathbb{C}^{I+1}, \, \boldsymbol{\mu} \neq \mathbf{0}, \text{ such that} \\ \boldsymbol{M}(k_h)\, \boldsymbol{\mu} = \mathbf{0}. \end{cases} \tag{6.32}$$

The elements $m_{ij}$ of the matrix $\boldsymbol{M}(k_h)$ are given, for $1 \leq i,j \leq I+1$, by

$$m_{ij} = \frac{1}{2}\big\langle (1+\mathcal{I}_0^h)\chi_j, \chi_i \big\rangle + \langle S_h(Z_h\chi_j), \chi_i \rangle - \langle D_h(\chi_j), \chi_i \rangle. \tag{6.33}$$

The desired resonances of the discretized system (6.32) are given by the values of $k_h$ for which the matrix $\boldsymbol{M}(k_h)$ becomes singular, i.e., non-invertible. Since the dependence on $k_h$ is highly non-linear (through the Green's function and eventually the impedance), it is in general not straightforward to find these resonances. One alternative is to consider, as

done by Durán et al. (2007*b*), the function of resonance-peaks

$$g_\lambda(k_h) = \frac{|\lambda_{\max}(k_h)|}{|\lambda_{\min}(k_h)|}, \tag{6.34}$$

where $\lambda_{\max}(k_h)$ and $\lambda_{\min}(k_h)$ denote respectively the biggest and smallest eigenvalues in modulus of the matrix $\boldsymbol{M}(k_h)$. This function possesses a countable amount of singularities in the complex plane, which correspond to the resonances. The computation of the eigenvalues can be performed by means of standard eigenvalue computation subroutines based on the QR-factorization (Anderson et al. 1999) or by means of power methods (cf., e.g., Burden & Faires 2001). Alternatively, instead of the eigenvalues we could also take into account in (6.34) the diagonal elements of the $\boldsymbol{U}$-matrix that stems from the LU-factorization of $\boldsymbol{M}(k_h)$, as done by Durán, Nédélec & Ossandón (2009).

To compute the resonant states or eigenstates associated to each resonance, we can take advantage of the knowledge of the eigenvector related with the smallest eigenvalue, e.g., obtained from some power method. If $k_h^*$ denotes a resonance, then $\boldsymbol{M}(k_h^*)$ becomes singular and $\lambda_{\min}(k_h^*) = 0$. The corresponding eigenstate $\boldsymbol{\mu}^*$ fulfills thus

$$\boldsymbol{M}(k_h^*)\,\boldsymbol{\mu}^* = \lambda_{\min}(k_h^*)\,\boldsymbol{\mu}^* = \boldsymbol{0}, \qquad \boldsymbol{\mu}^* \neq \boldsymbol{0}. \tag{6.35}$$

Consequently, it can be seen that the desired eigenstate $\boldsymbol{\mu}^*$ corresponds to the eigenvector of $\boldsymbol{M}(k_h^*)$ that is associated to $\lambda_{\min}(k_h^*)$.

## 6.4 Benchmark problem

### 6.4.1 Characteristic frequencies of the rectangle

As benchmark problem we consider the particular case of a rectangular harbor with a small opening. Resonances for a harbor of this kind are expected whenever the frequency of an incident wave is close to a characteristic frequency of the closed rectangle. To obtain the characteristic frequencies and oscillation modes of such a closed rectangle we have to solve first the problem

$$\begin{cases} \text{Find } k \in \mathbb{C} \text{ and } u : \Omega_r \to \mathbb{C},\ u \neq 0, \text{ such that} \\ \Delta u + k^2 u = 0 \qquad \text{in } \ \Omega_r, \\ \dfrac{\partial u}{\partial n} = 0 \qquad\quad \text{on } \ \Gamma_r, \end{cases} \tag{6.36}$$

where we denote the domain encompassed by the rectangle as $\Omega_r$ and its boundary as $\Gamma_r$. The unit normal $\boldsymbol{n}$ is taken outwardly oriented of $\Omega_r$. The rectangle is assumed to be of length $a$ and width $b$. The eigenfrequencies and eigenstates of the rectangle are well-known and can be determined analytically by using the method of variable separation. For this purpose we separate

$$u(\boldsymbol{x}) = v(x_1)w(x_2), \tag{6.37}$$

placing the origin at the lower left corner of the rectangle, as shown in Figure 6.2.

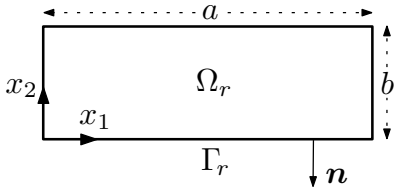


FIGURE 6.2. Closed rectangle.

Replacing now (6.37) in the Helmholtz equation, dividing by $vw$, and rearranging yields

$$-\frac{v''(x_1)}{v(x_1)} = \frac{w''(x_2)}{w(x_2)} + k^2. \tag{6.38}$$

Since both sides of the differential equation (6.38) depend on different variables, consequently they must be equal to a constant, denoted for convenience by $\kappa^2$, i.e.,

$$-\frac{v''(x_1)}{v(x_1)} = \frac{w''(x_2)}{w(x_2)} + k^2 = \kappa^2. \tag{6.39}$$

This way we obtain the two independent ordinary differential equations

$$v''(x_1) + \kappa^2 v(x_1) = 0, \tag{6.40}$$

$$w''(x_2) + (k^2 - \kappa^2) w(x_2) = 0. \tag{6.41}$$

The solutions of (6.40) and (6.41) are respectively of the form

$$v(x_1) = A_v \cos(\kappa x_1) + B_v \sin(\kappa x_1), \tag{6.42}$$

$$w(x_2) = A_w \cos\Big(\sqrt{k^2 - \kappa^2}\, x_2\Big) + B_w \sin\Big(\sqrt{k^2 - \kappa^2}\, x_2\Big), \tag{6.43}$$

where $A_v, B_v, A_w, B_w$ are constants to be determined. This is performed by means of the boundary condition in (6.36), which implies that

$$v'(0) = v'(a) = w'(0) = w'(b) = 0. \tag{6.44}$$

Since $v'(0) = w'(0) = 0$, thus $B_v = B_w = 0$. From the fact that $v'(a) = 0$ we get that $\kappa a = m\pi$ for $m \in \mathbb{Z}$. Hence

$$\kappa = \frac{m\pi}{a}. \tag{6.45}$$

On the other hand, $w'(b) = 0$ implies that $\sqrt{k^2 - \kappa^2}\, b = n\pi$ for $n \in \mathbb{Z}$. By rearranging and replacing (6.45) we obtain the real eigenfrequencies

$$k = \sqrt{\Big(\frac{m\pi}{a}\Big)^2 + \Big(\frac{n\pi}{b}\Big)^2}, \qquad m, n \in \mathbb{Z}. \tag{6.46}$$

The corresponding eigenstates, up to an arbitrary multiplicative constant, are then given by

$$u(\boldsymbol{x}) = \cos\Big(\frac{m\pi}{a} x_1\Big) \cos\Big(\frac{n\pi}{b} x_2\Big), \qquad m, n \in \mathbb{Z}. \tag{6.47}$$

For the particular case of a rectangle with length $a = 800$ and width $b = 400$, the characteristic frequencies are listed in Table 6.1.

TABLE 6.1. Eigenfrequencies of the rectangle in the range from $0$ to $0.02$.

| $m$ \ $n$ | 0 | 1 | 2 |
|---|---|---|---|
| 0 | 0.00000 | 0.00785 | 0.01571 |
| 1 | 0.00393 | 0.00878 | 0.01619 |
| 2 | 0.00785 | 0.01111 | 0.01756 |
| 3 | 0.01178 | 0.01416 | 0.01963 |
| 4 | 0.01571 | 0.01756 | |
| 5 | 0.01963 | | |

### 6.4.2 Rectangular harbor problem

We consider now the particular case when the domain $\Omega_e \subset \mathbb{R}^2_+$ is taken as a rectangular harbor with a small opening $d$, such as the domain depicted in Figure 6.3. We take for the rectangle a length $a = 800$, a width $b = 400$, and a small opening of size $d = 20$.

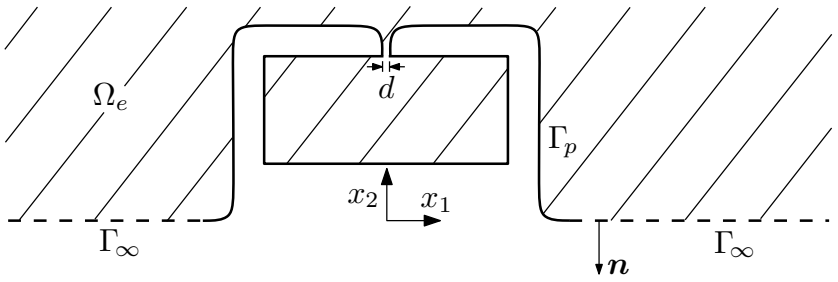


FIGURE 6.3. Rectangular harbor domain.

To simplify the problem, on $\Gamma_\infty$ we consider an impedance boundary condition with a constant impedance $Z_\infty = 0.02$ and on $\Gamma_p$ we take a Neumann boundary condition into account. The rectangular harbor problem can be thus stated as

$$\begin{cases} \text{Find } k \in \mathbb{C} \text{ and } u : \Omega_e \to \mathbb{C},\ u \neq 0, \text{ such that} \\ \Delta u + k^2 u = 0 & \text{in } \Omega_e, \\ \dfrac{\partial u}{\partial n} = 0 & \text{on } \Gamma_p, \\ -\dfrac{\partial u}{\partial n} + Z_\infty u = 0 & \text{on } \Gamma_\infty, \\ \text{+ Outgoing radiation condition as } |\boldsymbol{x}| \to \infty, \end{cases} \tag{6.48}$$

where the outgoing radiation condition is stated in (6.16).

The boundary curve $\Gamma_p$ is discretized into $I = 135$ segments with a discretization step $h = 40.4959$, as illustrated in Figure 6.4. The problem is solved computationally with finite boundary elements of type $\mathbb{P}_1$ by using subroutines programmed in Fortran 90, by

generating the mesh $\Gamma_p^h$ of the boundary with the free software Gmsh 2.4, and by representing graphically the results in Matlab 7.5 (R2007b). The eigenvalues of the matrix $\boldsymbol{M}(k_h)$, required to build the function of resonance-peaks (6.34), are computed by using the Lapack subroutines for complex nonsymmetric matrixes (cf. Anderson et al. 1999).

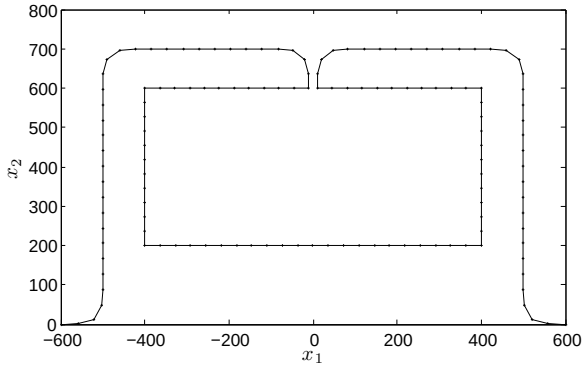


FIGURE 6.4. Mesh $\Gamma_p^h$ of the rectangular harbor.

The numerical results for the resonances, considering a step $\Delta k = 5 \cdot 10^{-5}$ between wave number samples, are illustrated in Figure 6.5. It can be observed that the peaks tend to coincide with the eigenfrequencies of the rectangle, which are represented by the dashed vertical lines. The first six oscillation modes are depicted in Figures 6.6, 6.7 & 6.8. Only the real parts are displayed, since the imaginary parts are close to zero. We remark that the first observed resonance corresponds to the so-called Helmholtz mode, since its associated eigenmode is constant.

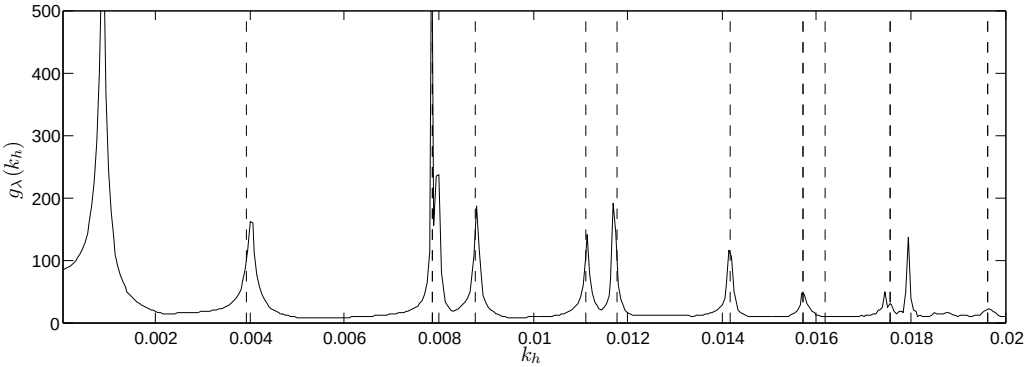


FIGURE 6.5. Resonances for the rectangular harbor.

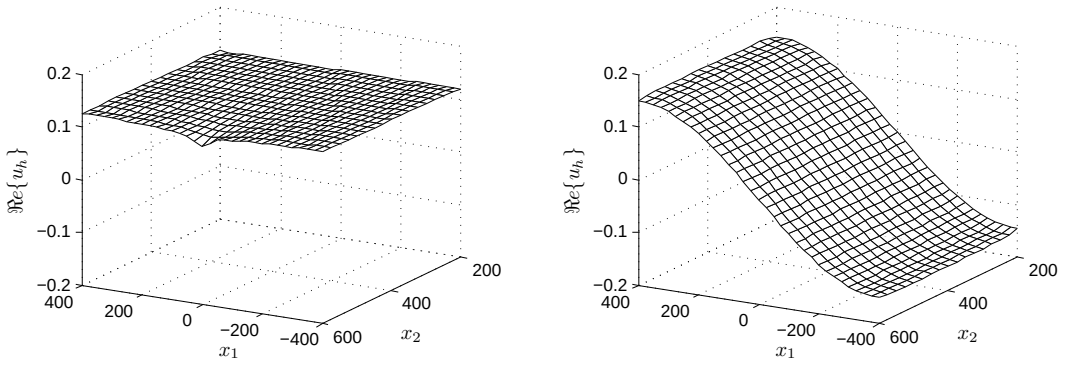


(a) $k_h = 0.000875$ (b) $k_h = 0.00393$

FIGURE 6.6. Oscillation modes: (a) Helmholtz mode; (b) Mode (1,0).

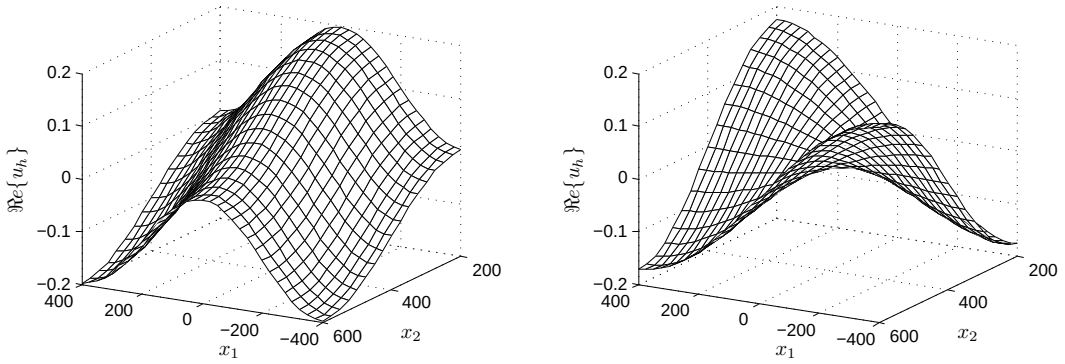


(a) $k_h = 0.00785$ (b) $k_h = 0.00878$

FIGURE 6.7. Oscillation modes: (a) Modes (0,1) and (2,0); (b) Mode (1,1).

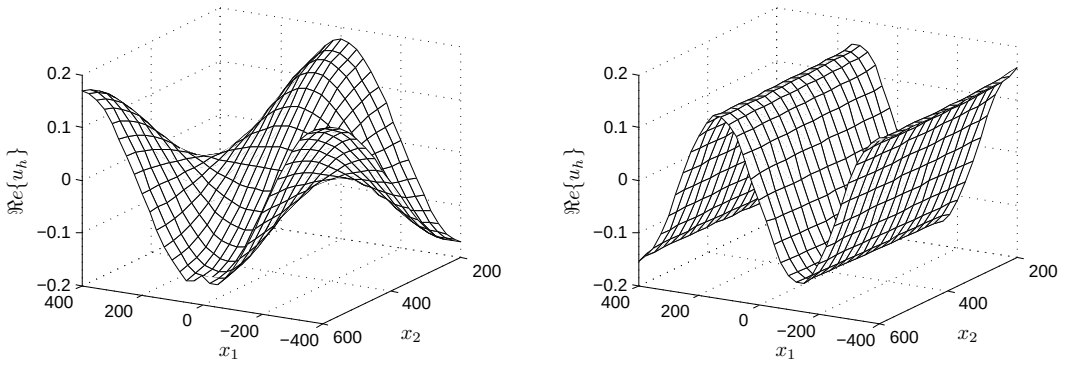


(a) $k_h = 0.01111$ (b) $k_h = 0.01178$

FIGURE 6.8. Oscillation modes: (a) Mode (2,1); (b) Mode (0,3).

# VII. OBLIQUE-DERIVATIVE HALF-PLANE LAPLACE PROBLEM

## 7.1 Introduction

In this chapter we apply the developed techniques to the computation of the Green's function for the oblique-derivative (impedance) half-plane Laplace problem.

We consider the problem of finding the Green's function for the Laplace equation in a two-dimensional half-plane with an oblique-derivative (impedance) boundary condition. Essentially, this Green's function describes outgoing oblique surface waves that emanate from a point source and which increase or decrease exponentially along the boundary, depending on the obliqueness of the derivative in the boundary condition.

An integral representation for this Green's function in half-spaces of three and higher dimensions was developed by Gilbarg & Trudinger (1983, page 121). Using an image method, it was later generalized by Keller (1981) to a wider class of equations, including the wave equation, the heat equation, and the Laplace equation. Its use for more general linear uniformly elliptic equations with discontinuous coefficients can be found in the articles of Di Fazio & Palagachev (1996) and Palagachev, Ragusa & Softova (2000). The generalization of this image method to wedges is performed by Gautesen (1988). When dealing with time-harmonic problems, this representation of the Green's function has to be supplied with an additional term to account for an outgoing surface-wave behavior, e.g., the terms (2.63) and (3.58) associated with the limiting absorption principle.

In the particular case when the oblique derivative becomes a normal derivative, we speak of a free-surface or impedance boundary condition, and the response to the point source is referred to as an infinite-depth free-surface Green's function, which is of great importance in linear water-wave theory (vid. Section A.10). An explicit representation for this Green's function in two dimensions was derived in Chapter II and its main relevance is that it allows to solve boundary value problems stated on compactly perturbed half-planes by using boundary integral equations and the boundary element method (Durán, Hein & Nédélec 2007*b*). Boundary layer potentials constructed by using Green's functions are also important for such different topics as proving solvability theorems and computing resonant states (Kuznetsov, Maz'ya & Vainberg 2002).

Poincaré was the first to state an oblique-derivative problem for a second-order elliptic partial differential operator in his studies on the theory of tides (Poincaré 1910). Since then, the so-called Poincaré problem has been the subject of many publications (cf. Egorov & Kondrat'ev 1969, Paneah 2000), and it arises naturally when determining the gravitational fields of celestial bodies. In this problem, the impedance of the boundary condition is taken as zero. Its main interest lies in the fact that it corresponds to a typical degenerate elliptic boundary value problem where the vector field of its solution is tangent to the boundary of the domain on some subset. The Poincaré problem for harmonic functions, in particular, arises in semiconductor physics and considers constant coefficients for the oblique derivative in the boundary condition (Krutitskii & Chikilev 2000). It allows to describe the Hall effect, i.e., when the direction of an electric current and the direction

of an electric field do not coincide in a semiconductor due the presence of a magnetic field (Krutitskii, Krutitskaya & Malysheva 1999). The two-dimensional Poincaré problem for the Laplace equation is treated in Lesnic (2007), Trefethen & Williams (1986), and further references can be also found in Lions (1956).

The main goal of this chapter is to derive rigorously an explicit representation for the half-plane Green's function of the Laplace equation with an oblique-derivative impedance boundary condition by extending and adapting the results obtained in Chapter II. Excepting the particular cases mentioned before, there has been no attempt to compute it explicitly. The aim is to express the Green's function in terms of a finite combination of known special and elementary functions, so as to be practical for numerical computation. It is also of interest to extend this representation, e.g., towards the complementary half-plane or by considering a complex impedance instead of a real one. There is likewise the interest of having adjusted expressions for the far field of the Green's function and to state the involved radiation condition accordingly.

The differential problem for the Green's function is stated in the upper half-plane and is defined in Section 7.2. In Section 7.3, the spectral Green's function is determined by using a partial Fourier transform along the horizontal axis. By computing its inverse Fourier transform, the desired spatial Green's function is then obtained in Section 7.4. Some properties and extensions of the Green's function are presented in Section 7.5, particularly its extension towards the lower half-plane and its extension to consider a complex impedance. The far field of the Green's function is determined in Section 7.6.

## 7.2 Green's function problem

We consider the radiation problem of oblique surface waves in the upper half-plane $\mathbb{R}^2_+ = \{\boldsymbol{y} \in \mathbb{R}^2 : y_2 > 0\}$ emanating from a fixed source point $\boldsymbol{x} \in \mathbb{R}^2_+$, as shown in Figure 7.1. The Green's function $G$ corresponds to the solution of this problem, computed in the sense of distributions for the variable $\boldsymbol{y}$ in the half-plane $\mathbb{R}^2_+$ by placing at the right-hand side of the Laplace equation a Dirac mass $\delta_{\boldsymbol{x}}$, which is located at $\boldsymbol{x}$. It is hence a solution $G(\boldsymbol{x}, \cdot) : \mathbb{R}^2_+ \to \mathbb{C}$ of

$$\Delta_{\boldsymbol{y}} G(\boldsymbol{x}, \boldsymbol{y}) = \delta_{\boldsymbol{x}}(\boldsymbol{y}) \qquad \text{in } \mathcal{D}'(\mathbb{R}^2_+), \tag{7.1a}$$

subject to the oblique-derivative impedance boundary condition

$$\frac{\partial G}{\partial s_{\boldsymbol{y}}}(\boldsymbol{x}, \boldsymbol{y}) + Z\, G(\boldsymbol{x}, \boldsymbol{y}) = 0 \qquad \text{on } \{y_2 = 0\}, \tag{7.1b}$$

where the oblique, skew, or directional derivative is given by

$$\frac{\partial G}{\partial s_{\boldsymbol{y}}}(\boldsymbol{x}, \boldsymbol{y}) = \boldsymbol{s} \cdot \nabla_{\boldsymbol{y}} G(\boldsymbol{x}, \boldsymbol{y}) = s_1 \frac{\partial G}{\partial y_1}(\boldsymbol{x}, \boldsymbol{y}) + s_2 \frac{\partial G}{\partial y_2}(\boldsymbol{x}, \boldsymbol{y}), \tag{7.1c}$$

and is taken in the direction of the vector

$$\boldsymbol{s} = (s_1, s_2) = (\cos\sigma,\, \sin\sigma), \qquad |\boldsymbol{s}| = \sqrt{s_1^2 + s_2^2} = 1. \tag{7.1d}$$

The boundary condition (7.1b) is expressed in terms of a real impedance $Z > 0$ and the unit vector $\boldsymbol{s}$ is constant and such that $s_2 > 0$, i.e., such that $0 < \sigma < \pi$. The case of complex $Z$ is discussed later in Section 7.5.

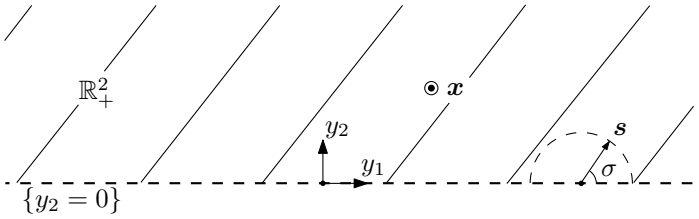


FIGURE 7.1. Domain of the Green's function problem.

To obtain outgoing oblique surface waves for the radiation problem and to ensure the uniqueness of its solution, an outgoing radiation condition has to be imposed additionally at infinity. We express it in its more adjusted form, as in (2.17), which is later justified from the far field of the Green's function, developed in Section 7.6. The outgoing radiation condition is given, as $|\boldsymbol{y}| \to \infty$, by

$$|G| \le \frac{C}{|\boldsymbol{y}|} \quad \text{and} \quad \left|\frac{\partial G}{\partial |\boldsymbol{y}|}\right| \le \frac{C}{|\boldsymbol{y}|^2} \qquad \text{if } \boldsymbol{y}\cdot\boldsymbol{s} > \frac{1}{Z}\ln\bigl(1 + Z\pi|\boldsymbol{y}|\bigr), \tag{7.1e}$$

$$|G| \le Ce^{-Z\boldsymbol{y}\cdot\boldsymbol{s}} \quad \text{and} \quad \left|\frac{\partial G}{\partial |\boldsymbol{y}\times\boldsymbol{s}|} - iZG\right| \le \frac{Ce^{-Z\boldsymbol{y}\cdot\boldsymbol{s}}}{|\boldsymbol{y}\times\boldsymbol{s}|} \qquad \text{if } \boldsymbol{y}\cdot\boldsymbol{s} < \frac{1}{Z}\ln\bigl(1 + Z\pi|\boldsymbol{y}|\bigr), \tag{7.1f}$$

for some constants $C > 0$, which are independent of $\boldsymbol{y}$, and where

$$\boldsymbol{y}\cdot\boldsymbol{s} = s_1y_1 + s_2y_2 \qquad \text{and} \qquad \boldsymbol{y}\times\boldsymbol{s} = s_2y_1 - s_1y_2. \tag{7.2}$$

This radiation condition specifies two regions of different asymptotic behaviors for the Green's function, analogously as shown in Figure 2.2. Both behaviors are separated by rotated logarithmic curves. Above and away from the line $\boldsymbol{y}\cdot\boldsymbol{s} = 0$, the behavior (7.1e) dominates, which is related to the asymptotic decaying of the fundamental solution for the Laplace equation. Below and near the line $\boldsymbol{y}\cdot\boldsymbol{s} = 0$, on the other hand, the behavior (7.1f) resembles a Sommerfeld radiation condition, and is therefore associated to surface waves propagating in an oblique direction, i.e., to oblique surface waves. Along the boundary $\{y_2 = 0\}$, these waves decrease or increase exponentially, and their real and imaginary parts have the same amplitude.

To solve the Green's function problem (7.1), we separate its solution $G$ into a homogeneous and a particular part, namely $G = G_H + G_P$. The homogeneous solution $G_H$, appropriately scaled, corresponds to the additional term that is required to ensure an appropriate outgoing behavior for the oblique surface waves. In the particular case when the oblique derivative becomes normal, as in Chapter II, then a limiting absorption principle

can be used to explain its presence. The solution $G_H$ of the homogeneous problem, i.e., of (7.1*a–b*) without the Dirac mass, can be conveniently expressed as

$$G_H(\boldsymbol{x},\boldsymbol{y}) = \alpha\, e^{-Z(s_2+is_1)(v_2-iv_1)} + \beta\, e^{-Z(s_2-is_1)(v_2+iv_1)}, \tag{7.3}$$

where the notation

$$v_1 = y_1 - x_1 \qquad \text{and} \qquad v_2 = y_2 + x_2 \tag{7.4}$$

is used. The constants $\alpha, \beta \in \mathbb{C}$ in (7.3) are arbitrary and may depend on $\boldsymbol{x}$. These constants are fixed later on by means of the radiation condition, once the particular solution $G_P$ of (7.1) has been better determined.

## 7.3 Spectral Green's function

### 7.3.1 Spectral boundary-value problem

The particular solution $G_P$ satisfies (7.1*a–b*) and has to remain bounded as $y_2 \to \infty$. To compute it, we use a modified partial Fourier transform on the horizontal $y_1$-axis, taking advantage of the fact that there is no horizontal variation in the geometry of the problem. We define the Fourier transform of a function $F\big(\boldsymbol{x},(\cdot,y_2)\big) : \mathbb{R} \to \mathbb{C}$ by

$$\widehat{F}(\xi; y_2, x_2) = \frac{1}{\sqrt{2\pi}} \int_{-\infty}^{\infty} F(\boldsymbol{x},\boldsymbol{y})\, e^{-i\xi(y_1-x_1)}\, \mathrm{d}y_1, \qquad \xi \in \mathbb{R}. \tag{7.5}$$

Applying the Fourier transform (7.5) on (7.1*a–b*) leads to a second-order boundary-value problem for the variable $y_2$, given by

$$\frac{\partial^2 \widehat{G}_P}{\partial y_2^2}(\xi) - \xi^2 \widehat{G}_P(\xi) = \frac{\delta(y_2 - x_2)}{\sqrt{2\pi}}, \qquad y_2 > 0, \tag{7.6a}$$

$$s_2 \frac{\partial \widehat{G}_P}{\partial y_2}(\xi) + \big(is_1\xi + Z\big)\widehat{G}_P(\xi) = 0, \qquad y_2 = 0. \tag{7.6b}$$

We use undetermined coefficients and solve the differential equation (7.6a) respectively in the strip $\{\boldsymbol{y} \in \mathbb{R}^2_+ \,:\, 0 < y_2 < x_2\}$ and in the half-plane $\{\boldsymbol{y} \in \mathbb{R}^2_+ \,:\, y_2 > x_2\}$. This gives a solution for $\widehat{G}_P$ in each domain, as a linear combination of two independent solutions of an ordinary differential equation, namely

$$\widehat{G}_P(\xi) = \begin{cases} a\, e^{|\xi| y_2} + b\, e^{-|\xi| y_2} & \text{for } \ 0 < y_2 < x_2, \\ c\, e^{|\xi| y_2} + d\, e^{-|\xi| y_2} & \text{for } \ y_2 > x_2. \end{cases} \tag{7.7}$$

The unknowns $a$, $b$, $c$, and $d$, which depend on $\xi$ and $x_2$, are determined through the boundary condition and by considering continuity and the behavior at infinity.

### 7.3.2 Particular spectral Green's function

Now, thanks to (7.7), the computation of $\widehat{G}_P$ is straightforward. From (7.6b) a relation for the coefficients $a$ and $b$ can be derived, which is given by

$$a\big(Z + s_2|\xi| + is_1\xi\big) + b\big(Z - s_2|\xi| + is_1\xi\big) = 0. \tag{7.8}$$

Since the solution (7.7) has to remain bounded at infinity as $y_2 \to \infty$, it follows that

$$c = 0. \tag{7.9}$$

To ensure continuity for the Green's function at the point $y_2 = x_2$, it is needed that

$$d = a\, e^{|\xi| 2x_2} + b. \tag{7.10}$$

Using relations (7.8), (7.9), and (7.10) in (7.7), we obtain the expression

$$\widehat{G}_P(\xi) = a\, e^{|\xi| x_2} \left[ e^{-|\xi||y_2 - x_2|} - \left( \frac{Z + s_2|\xi| + i s_1 \xi}{Z - s_2|\xi| + i s_1 \xi} \right) e^{-|\xi|(y_2 + x_2)} \right]. \tag{7.11}$$

By computing the second derivative of (7.11) in the sense of distributions and by replacing it in (7.6a), we obtain that

$$a = -\frac{e^{-|\xi| x_2}}{\sqrt{8\pi}\,|\xi|}. \tag{7.12}$$

Finally, the particular spectral Green's function $\widehat{G}_P$ is given by

$$\widehat{G}_P(\xi; y_2, x_2) = -\frac{e^{-|\xi||y_2 - x_2|}}{\sqrt{8\pi}\,|\xi|} + \left( \frac{Z + s_2|\xi| + i s_1 \xi}{Z - s_2|\xi| + i s_1 \xi} \right) \frac{e^{-|\xi|(y_2 + x_2)}}{\sqrt{8\pi}\,|\xi|}. \tag{7.13}$$

### 7.3.3 Analysis of singularities

We have to analyze now the singularities of the particular spectral Green's function $\widehat{G}_P$, so as to obtain its asymptotic behavior and thus determine the constants $\alpha, \beta$ of the homogeneous solution (7.3). For this purpose, we extend the Fourier variable towards the complex domain, i.e., $\xi \in \mathbb{C}$, in which case the absolute value $|\xi|$ has to be understood as the square root $\sqrt{\xi^2}$, where $-\pi/2 < \arg\sqrt{\xi^2} \leq \pi/2$, that is, always the root with the nonnegative real part is taken. This square root presents two branch cuts, which are located respectively on the positive and on the negative imaginary axis of $\xi$. The particular spectral Green's function $\widehat{G}_P$, for $\xi \in \mathbb{C}$, becomes therefore

$$\widehat{G}_P(\xi) = -\frac{e^{-\sqrt{\xi^2}\,|y_2 - x_2|}}{\sqrt{8\pi}\,\sqrt{\xi^2}} + \left( \frac{Z + s_2\sqrt{\xi^2} + i s_1 \xi}{Z - s_2\sqrt{\xi^2} + i s_1 \xi} \right) \frac{e^{-\sqrt{\xi^2}\,(y_2 + x_2)}}{\sqrt{8\pi}\,\sqrt{\xi^2}}. \tag{7.14}$$

This function is continuous on $\xi$ along the real axis and it incorporates a removable singularity at $\xi = 0$, in the same manner as shown in Section 2.3. The function $\widehat{G}_P$ has also branch cuts on the positive and negative imaginary axis. Finally, (7.14) presents two simple poles at $\xi = Z(s_2 + i s_1)$ and $\xi = -Z(s_2 - i s_1)$, whose residues are characterized by

$$\lim_{\xi \to \pm Z(s_2 \pm i s_1)} \big( \xi \mp Z(s_2 \pm i s_1) \big)\, \widehat{G}_P(\xi) = \mp \frac{s_2}{\sqrt{2\pi}} (s_2 \pm i s_1) e^{-Z(s_2 \pm i s_1) v_2}. \tag{7.15}$$

Otherwise the function $\widehat{G}_P$ is regular and continuous. To analyze the effect of the poles, we study at first the inverse Fourier transform of

$$\widehat{P}(\xi) = -\frac{s_2}{\sqrt{2\pi}} (s_2 + i s_1) \frac{e^{-Z(s_2 + i s_1) v_2}}{\xi - Z(s_2 + i s_1)} + \frac{s_2}{\sqrt{2\pi}} (s_2 - i s_1) \frac{e^{-Z(s_2 - i s_1) v_2}}{\xi + Z(s_2 - i s_1)}. \tag{7.16}$$

This can be achieved by considering the Fourier transform of the sign function, i.e.,

$$\operatorname{sign}(v_1) \qquad \xrightarrow{\mathcal{F}} \qquad -i\sqrt{\frac{2}{\pi}}\frac{1}{\xi}, \tag{7.17}$$

whose right-hand side is to be interpreted in the sense of the principal value, and by using the translation, scaling, and linearity properties of the Fourier transform, as much in the spatial as in the spectral domain (cf., e.g., Gasquet & Witomski 1999). The inverse Fourier transform of (7.16) is then given by

$$\begin{aligned} P(\boldsymbol{x},\boldsymbol{y}) = & -i\frac{s_2}{2}(s_2+is_1)\operatorname{sign}(v_1)\, e^{-Z(s_2v_2+s_1v_1)}e^{iZ(s_2v_1-s_1v_2)} \\ & +i\frac{s_2}{2}(s_2-is_1)\operatorname{sign}(v_1)\, e^{-Z(s_2v_2+s_1v_1)}e^{-iZ(s_2v_1-s_1v_2)}. \end{aligned} \tag{7.18}$$

The exponential terms in (7.18) are compatible with the asymptotic behavior of the Green's function, as will be seen later, but the one-dimensional nature of the Fourier transform does not allow to retrieve correctly the direction of the cut that is present due the $\operatorname{sign}$ function. Instead of being vertical along the $v_2$-axis as in (7.18), the direction of this cut has to coincide with the oblique vector $\boldsymbol{s}$ in the $(v_1, v_2)$-plane. To account for this issue we can consider, instead of (7.16), the expression

$$\begin{aligned} \widehat{Q}(\xi) = & -\frac{s_2}{\sqrt{2\pi}}(s_2+is_1)\, e^{-i\frac{s_1}{s_2}v_2(\xi-Z(s_2+is_1))}\frac{e^{-Z(s_2+is_1)v_2}}{\xi-Z(s_2+is_1)} \\ & +\frac{s_2}{\sqrt{2\pi}}(s_2-is_1)\, e^{-i\frac{s_1}{s_2}v_2(\xi+Z(s_2-is_1))}\frac{e^{-Z(s_2-is_1)v_2}}{\xi+Z(s_2-is_1)}, \end{aligned} \tag{7.19}$$

which also describes correctly the residues of the poles, but incorporating an additional exponential behavior that treats properly the $v_2$-variable. We remark that this additional exponential factor becomes unity when $s_1 = 0$, i.e., when the oblique derivative becomes normal. By using again (7.17) and the same properties of the Fourier transform as before, we obtain that the inverse Fourier transform of (7.19) is readily given by

$$\begin{aligned} Q(\boldsymbol{x},\boldsymbol{y}) = & -i\frac{s_2}{2}(s_2+is_1)\operatorname{sign}(s_2v_1-s_1v_2)\, e^{-Z(s_2v_2+s_1v_1)}e^{iZ(s_2v_1-s_1v_2)} \\ & +i\frac{s_2}{2}(s_2-is_1)\operatorname{sign}(s_2v_1-s_1v_2)\, e^{-Z(s_2v_2+s_1v_1)}e^{-iZ(s_2v_1-s_1v_2)}. \end{aligned} \tag{7.20}$$

Now the cut due the $\operatorname{sign}$ function coincides correctly with the oblique vector $\boldsymbol{s}$ and retrieves appropriately the asymptotic behavior of the oblique surface waves.

It can be observed that (7.20) describes the asymptotic behavior of stationary oblique surface waves, since its imaginary part is zero. In order to obtain an outgoing-wave behavior, this missing imaginary part is provided by the homogeneous solution (7.3), which has to be scaled according to

$$\begin{aligned} G_H(\boldsymbol{x},\boldsymbol{y}) = & -i\frac{s_2}{2}(s_2+is_1)\, e^{-Z(s_2v_2+s_1v_1)}e^{iZ(s_2v_1-s_1v_2)} \\ & -i\frac{s_2}{2}(s_2-is_1)\, e^{-Z(s_2v_2+s_1v_1)}e^{-iZ(s_2v_1-s_1v_2)}. \end{aligned} \tag{7.21}$$

The Fourier transform of (7.21) contains two Dirac masses and is given by

$$\begin{aligned}\widehat{G}_H(\xi; y_2, x_2) = &- i\sqrt{\frac{\pi}{2}}\, s_2(s_2 + is_1)\, e^{-Z(s_2+is_1)v_2}\, \delta\big(\xi - Z(s_2 + is_1)\big) \\ &- i\sqrt{\frac{\pi}{2}}\, s_2(s_2 - is_1)\, e^{-Z(s_2-is_1)v_2}\, \delta\big(\xi + Z(s_2 - is_1)\big). \end{aligned} \tag{7.22}$$

### 7.3.4 Complete spectral Green's function

The complete spectral Green's function, decomposed as $\widehat{G} = \widehat{G}_P + \widehat{G}_H$, is thus obtained by adding the particular solution (7.13) and the homogeneous solution (7.22), which yields

$$\begin{aligned}\widehat{G}(\xi; y_2, x_2) = &- \frac{e^{-|\xi||y_2 - x_2|}}{\sqrt{8\pi}\,|\xi|} + \left(\frac{Z + s_2|\xi| + is_1\xi}{Z - s_2|\xi| + is_1\xi}\right) \frac{e^{-|\xi|(y_2+x_2)}}{\sqrt{8\pi}\,|\xi|} \\ &- i\sqrt{\frac{\pi}{2}}\, s_2(s_2 + is_1)\, e^{-Z(s_2+is_1)(y_2+x_2)} \delta\big(\xi - Z(s_2 + is_1)\big) \\ &- i\sqrt{\frac{\pi}{2}}\, s_2(s_2 - is_1)\, e^{-Z(s_2-is_1)(y_2+x_2)} \delta\big(\xi + Z(s_2 - is_1)\big). \end{aligned} \tag{7.23}$$

For our further analysis, we decompose the particular solution (7.13) into three terms, namely $\widehat{G}_P = \widehat{G}_\infty + \widehat{G}_D + \widehat{G}_R$, where

$$\widehat{G}_\infty(\xi; y_2, x_2) = -\frac{e^{-|\xi||y_2 - x_2|}}{\sqrt{8\pi}\,|\xi|}, \tag{7.24}$$

$$\widehat{G}_D(\xi; y_2, x_2) = \frac{e^{-|\xi|(y_2+x_2)}}{\sqrt{8\pi}\,|\xi|}, \tag{7.25}$$

$$\widehat{G}_R(\xi; y_2, x_2) = \frac{s_2\, e^{-|\xi|(y_2+x_2)}}{\sqrt{2\pi}\,\big(Z - s_2|\xi| + is_1\xi\big)}. \tag{7.26}$$

## 7.4 Spatial Green's function

### 7.4.1 Decomposition

The particular spatial Green's function $G_P$ is given by the inverse Fourier transform of (7.13), namely by

$$\begin{aligned}G_P(\boldsymbol{x}, \boldsymbol{y}) = &- \frac{1}{4\pi}\int_{-\infty}^{\infty} \frac{e^{-|\xi||y_2 - x_2|}}{|\xi|}\, e^{i\xi(y_1 - x_1)} \mathrm{d}\xi \\ &+ \frac{1}{4\pi}\int_{-\infty}^{\infty} \left(\frac{Z + s_2|\xi| + is_1\xi}{Z - s_2|\xi| + is_1\xi}\right) \frac{e^{-|\xi|(y_2+x_2)}}{|\xi|}\, e^{i\xi(y_1 - x_1)} \mathrm{d}\xi. \end{aligned} \tag{7.27}$$

Due the linearity of the Fourier transform, the decomposition $G_P = G_\infty + G_D + G_R$ holds also in the spatial domain. We compute now each term in an independent manner and add the results at the end.

### 7.4.2 Term of the full-plane Green's function

The first term in (7.27) corresponds to the inverse Fourier transform of (7.24), and can be rewritten as

$$G_\infty(\boldsymbol{x},\boldsymbol{y}) = -\frac{1}{2\pi}\int_0^\infty \frac{e^{-\xi|y_2-x_2|}}{\xi}\cos\big(\xi(y_1-x_1)\big)\mathrm{d}\xi. \tag{7.28}$$

This integral is divergent in the classical sense (cf., e.g., Gradshteyn & Ryzhik 2007, equation 3.941–2) and yields, as for (2.75), the full-plane Green's function of the Laplace equation, namely

$$G_\infty(\boldsymbol{x},\boldsymbol{y}) = \frac{1}{2\pi}\ln|\boldsymbol{y}-\boldsymbol{x}|. \tag{7.29}$$

### 7.4.3 Term associated with a Dirichlet boundary condition

The inverse Fourier transform of (7.25) is obtained in the same manner as the term $G_\infty$. In this case we have that

$$G_D(\boldsymbol{x},\boldsymbol{y}) = \frac{1}{2\pi}\int_0^\infty \frac{e^{-\xi(y_2+x_2)}}{\xi}\cos\big(\xi(y_1-x_1)\big)\mathrm{d}\xi, \tag{7.30}$$

which implies that

$$G_D(\boldsymbol{x},\boldsymbol{y}) = -\frac{1}{2\pi}\ln|\boldsymbol{y}-\bar{\boldsymbol{x}}|, \tag{7.31}$$

being $\bar{\boldsymbol{x}} = (x_1,-x_2)$ the image point of $\boldsymbol{x}$ in the lower half-plane. It represents the additional term that appears in the Green's function due the method of images when considering a Dirichlet boundary condition.

### 7.4.4 Remaining term

The remaining term $G_R$, the inverse Fourier transform of (7.26), can be expressed as

$$G_R(\boldsymbol{x},\boldsymbol{y}) = \frac{s_2}{2\pi}\int_{-\infty}^\infty \frac{e^{-|\xi|v_2}}{Z-s_2|\xi|+is_1\xi}\,e^{i\xi v_1}\,\mathrm{d}\xi. \tag{7.32}$$

Separating positive and negative values of $\xi$ in the integral and rearranging, yields

$$\begin{aligned} G_R(\boldsymbol{x},\boldsymbol{y}) = {}& \frac{s_2}{2\pi}(s_2+is_1)\int_0^\infty \frac{e^{-\xi(v_2-iv_1)}}{Z(s_2+is_1)-\xi}\,\mathrm{d}\xi \\ & + \frac{s_2}{2\pi}(s_2-is_1)\int_0^\infty \frac{e^{-\xi(v_2+iv_1)}}{Z(s_2-is_1)-\xi}\,\mathrm{d}\xi. \end{aligned} \tag{7.33}$$

By performing respectively in the first and second integrals of (7.33) the change of variable $\eta = (v_2-iv_1)\big(\xi - Z(s_2+is_1)\big)$ and $\eta = (v_2+iv_1)\big(\xi - Z(s_2-is_1)\big)$, we obtain

$$\begin{aligned} G_R(\boldsymbol{x},\boldsymbol{y}) = {}& \frac{s_2}{2\pi}(s_2+is_1)\,e^{-Z\boldsymbol{v}\cdot\boldsymbol{s}+iZ\boldsymbol{v}\times\boldsymbol{s}}\,\mathrm{Ei}\big(Z\boldsymbol{v}\cdot\boldsymbol{s}-iZ\boldsymbol{v}\times\boldsymbol{s}\big) \\ & + \frac{s_2}{2\pi}(s_2-is_1)\,e^{-Z\boldsymbol{v}\cdot\boldsymbol{s}-iZ\boldsymbol{v}\times\boldsymbol{s}}\,\mathrm{Ei}\big(Z\boldsymbol{v}\cdot\boldsymbol{s}+iZ\boldsymbol{v}\times\boldsymbol{s}\big), \end{aligned} \tag{7.34}$$

where we use the notation

$$\boldsymbol{v}\cdot\boldsymbol{s} = s_2v_2+s_1v_1 \qquad \text{and} \qquad \boldsymbol{v}\times\boldsymbol{s} = s_2v_1-s_1v_2, \tag{7.35}$$

and where Ei denotes the exponential integral function (vid. Subsection A.2.3). This special function is defined as a Cauchy principal value by

$$\mathrm{Ei}(z) = -\fint_{-z}^{\infty} \frac{e^{-t}}{t}\,\mathrm{d}t = \fint_{-\infty}^{z} \frac{e^{t}}{t}\,\mathrm{d}t \qquad \big(|\arg z| < \pi\big), \tag{7.36}$$

and it can be characterized in the whole complex plane through the series expansion

$$\mathrm{Ei}(z) = \gamma + \ln z + \sum_{n=1}^{\infty} \frac{z^n}{n\,n!} \qquad \big(|\arg z| < \pi\big), \tag{7.37}$$

where $\gamma$ denotes Euler's constant and where the principal value of the logarithm is taken, i.e., the branch cut runs along the negative real axis. Its derivative is

$$\frac{\mathrm{d}}{\mathrm{d}z}\,\mathrm{Ei}(z) = \frac{e^z}{z}. \tag{7.38}$$

For large arguments, as $x \to \infty$ along the real line and as $|y| \to \infty$ along the imaginary axis, the exponential integral admits the asymptotic divergent series expansions

$$\mathrm{Ei}(x) = \frac{e^x}{x} \sum_{n=0}^{\infty} \frac{n!}{x^n} \qquad (x > 0), \tag{7.39}$$

$$\mathrm{Ei}(iy) = i\pi\,\mathrm{sign}(y) + \frac{e^{iy}}{iy} \sum_{n=0}^{\infty} \frac{n!}{(iy)^n} \qquad (y \in \mathbb{R}). \tag{7.40}$$

### 7.4.5 Complete spatial Green's function

The complete spatial Green's function is finally obtained by adding the terms (7.22), (7.29), (7.31), and (7.34), and is thus given explicitly by

$$\begin{aligned} G(\boldsymbol{x},\boldsymbol{y}) = {} & \frac{1}{2\pi}\ln|\boldsymbol{y}-\boldsymbol{x}| - \frac{1}{2\pi}\ln|\boldsymbol{y}-\bar{\boldsymbol{x}}| \\ & + \frac{s_2}{2\pi}(s_2 + is_1)\,e^{-Z\boldsymbol{v}\cdot\boldsymbol{s}+iZ\boldsymbol{v}\times\boldsymbol{s}}\Big(\mathrm{Ei}\big(Z\boldsymbol{v}\cdot\boldsymbol{s} - iZ\boldsymbol{v}\times\boldsymbol{s}\big) - i\pi\Big) \\ & + \frac{s_2}{2\pi}(s_2 - is_1)\,e^{-Z\boldsymbol{v}\cdot\boldsymbol{s}-iZ\boldsymbol{v}\times\boldsymbol{s}}\Big(\mathrm{Ei}\big(Z\boldsymbol{v}\cdot\boldsymbol{s} + iZ\boldsymbol{v}\times\boldsymbol{s}\big) - i\pi\Big), \end{aligned} \tag{7.41}$$

where $\bar{\boldsymbol{x}} = (x_1, -x_2)$ and where the notations (7.4) and (7.35) are used.

The numerical evaluation of the Green's function (7.41) can be performed straightforwardly in Mathematica, by using the function `ExpIntegralEi`, and almost directly in Fortran, by adapting the computational subroutines described in Morris (1993) or, alternatively, the algorithm delineated in Amos (1990*a*,*b*). Great care has to be taken in the latter case, though, with the correct definition of the exponential integral, and particularly with the analytic branch cut. The case for $Z = 1$, $\sigma = 5\pi/11$, and $\boldsymbol{x} = (0, 2)$ is illustrated in Figures 7.2 & 7.3.

## 7.5 Extension and properties

The spatial Green's function can be extended in a locally analytic way towards the full-plane $\mathbb{R}^2$ in a straightforward and natural manner, just by considering the expression (7.41)

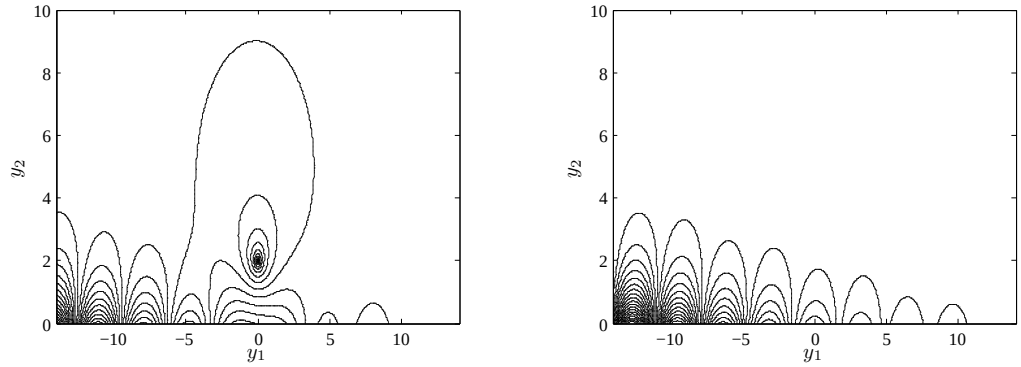


(a) Real part (b) Imaginary part

FIGURE 7.2. Contour plot of the complete spatial Green's function.

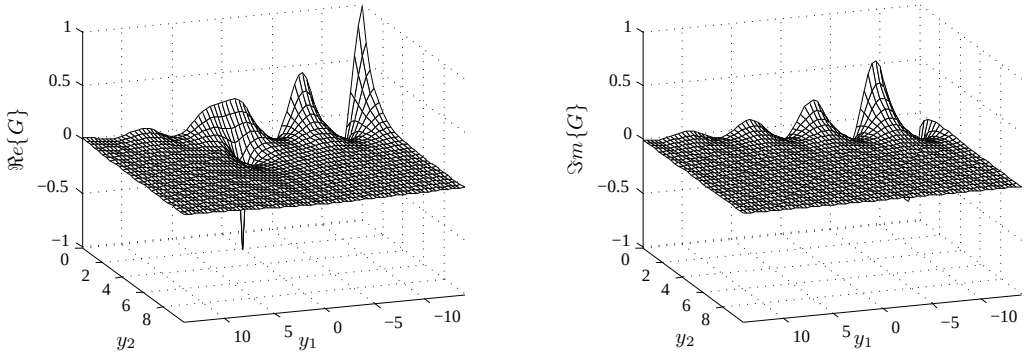


(a) Real part (b) Imaginary part

FIGURE 7.3. Oblique view of the complete spatial Green's function.

valid for all $\boldsymbol{x}, \boldsymbol{y} \in \mathbb{R}^2$, instead of just for $\mathbb{R}^2_+$. This extension has two singularities of logarithmic type at the points $\boldsymbol{x}$ and $\bar{\boldsymbol{x}}$, whose behavior is characterized by

$$G(\boldsymbol{x}, \boldsymbol{y}) \sim \frac{1}{2\pi} \ln |\boldsymbol{y} - \boldsymbol{x}|, \qquad \boldsymbol{y} \longrightarrow \boldsymbol{x}, \tag{7.42}$$

$$G(\boldsymbol{x}, \boldsymbol{y}) \sim \left( \frac{2s_2 - 1}{2\pi} \right) \ln |\boldsymbol{y} - \bar{\boldsymbol{x}}|, \qquad \boldsymbol{y} \longrightarrow \bar{\boldsymbol{x}}. \tag{7.43}$$

Across the half-line $\Upsilon = \{\boldsymbol{y} \in \mathbb{R}^2 : \boldsymbol{y} = \bar{\boldsymbol{x}} - \alpha \boldsymbol{s}, \ \alpha > 0\}$, as shown in Figure 7.4, a jump appears for the Green's function due the analytic branch cut of the exponential integral functions, which is given by

$$K(\boldsymbol{x}, \boldsymbol{y}) = G|_+ - G|_- = 2s_1 s_2 \, e^{-Z(s_2 v_2 + s_1 v_1)}. \tag{7.44}$$

For the same reason, there exists also a jump for the perpendicular oblique derivative across $\Upsilon$, which is represented by

$$J(\boldsymbol{x},\boldsymbol{y}) = \left.\frac{\partial G}{\partial t_{\boldsymbol{y}}}\right|_{+} - \left.\frac{\partial G}{\partial t_{\boldsymbol{y}}}\right|_{-} = 2Z s_2^2\, e^{-Z(s_2 v_2 + s_1 v_1)}, \tag{7.45}$$

where $\partial G/\partial t_{\boldsymbol{y}} = \boldsymbol{t}\cdot\nabla_{\boldsymbol{y}} G$, being $\boldsymbol{t} = (s_2, -s_1)$.

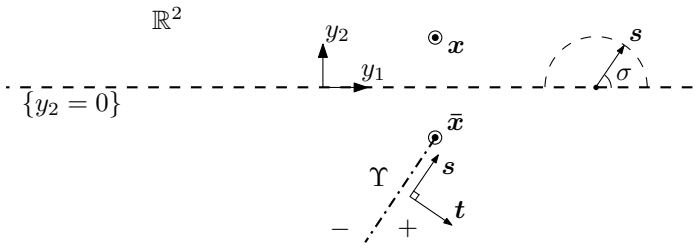


FIGURE 7.4. Domain of the extended Green's function.

As long as $x_2 \neq 0$ the boundary condition (7.1b) continues to be homogeneous. Nonetheless, if the source point $\boldsymbol{x}$ lies on the half-plane's boundary, i.e., if $x_2 = 0$, then the boundary condition ceases to be homogeneous in the sense of distributions. This can be deduced from (7.22) and (7.27) by verifying that

$$\lim_{y_2\to 0^+}\left\{\frac{\partial G}{\partial s_{\boldsymbol{y}}}\big((x_1,0),\boldsymbol{y}\big) + Z\,G\big((x_1,0),\boldsymbol{y}\big)\right\} = s_2\,\delta_{x_1}(y_1). \tag{7.46}$$

To illustrate more clearly the contribution of each logarithmic singularity to the Dirac mass in the boundary condition, which holds only on $\{y_2 = 0\}$, we express the right-hand side of (7.46) as

$$s_2\,\delta_{x_1}(y_1) = \frac{1}{2}\,\delta_{\boldsymbol{x}}(\boldsymbol{y}) + \left(s_2 - \frac{1}{2}\right)\delta_{\bar{\boldsymbol{x}}}(\boldsymbol{y}). \tag{7.47}$$

It can be seen now that the Green's function extended in the abovementioned way satisfies, for $\boldsymbol{x} \in \mathbb{R}^2$, in the sense of distributions, and instead of (7.1), the problem of finding $G(\boldsymbol{x},\cdot) : \mathbb{R}^2 \to \mathbb{C}$ such that

$$\Delta_{\boldsymbol{y}} G = \delta_{\boldsymbol{x}} + (2s_2 - 1)\,\delta_{\bar{\boldsymbol{x}}} + J\delta_{\Upsilon} + K\frac{\partial \delta_{\Upsilon}}{\partial t} \qquad \text{in } \mathcal{D}'(\mathbb{R}^2), \tag{7.48a}$$

$$\frac{\partial G}{\partial s_{\boldsymbol{y}}} + Z\,G = \frac{1}{2}\,\delta_{\boldsymbol{x}} + \left(s_2 - \frac{1}{2}\right)\delta_{\bar{\boldsymbol{x}}} \qquad \text{on } \{y_2 = 0\}, \tag{7.48b}$$

and such that the radiation condition (7.1*e–f*) is satisfied as $|\boldsymbol{y}| \to \infty$ for $\boldsymbol{y} \in \mathbb{R}^2_+$, where $\delta_{\Upsilon}$ denotes a Dirac-mass distribution along the $\Upsilon$-curve.

We note that the half-plane Green's function (7.41) is not symmetric in $\boldsymbol{x}$ and $\boldsymbol{y}$ in the general case since the differential operator is not self-adjoint, but it holds that

$$G(\boldsymbol{x},\boldsymbol{y}) = G(-\bar{\boldsymbol{y}}, -\bar{\boldsymbol{x}}) \qquad \forall \boldsymbol{x},\boldsymbol{y} \in \mathbb{R}^2, \tag{7.49}$$

where again $\bar{\boldsymbol{x}} = (x_1, -x_2)$ and $\bar{\boldsymbol{y}} = (y_1, -y_2)$.

When the oblique derivative becomes a normal derivative, i.e., when $s_2 = 1$, then the expression (7.41) effectively corresponds to the infinite-depth free-surface Green's function expressed in (2.94).

Another property is that we retrieve with (7.41) the special case of a homogenous Dirichlet boundary condition in $\mathbb{R}^2_+$ when $Z \to \infty$, namely

$$G(\boldsymbol{x}, \boldsymbol{y}) = \frac{1}{2\pi} \ln |\boldsymbol{y} - \boldsymbol{x}| - \frac{1}{2\pi} \ln |\boldsymbol{y} - \bar{\boldsymbol{x}}|. \tag{7.50}$$

The same Green's function (7.50) is also obtained when $s_2 = 0$. Likewise, we retrieve with (7.41) the special case of the Poincaré problem in $\mathbb{R}^2_+$ when $Z \to 0$, i.e.,

$$\begin{aligned} G(\boldsymbol{x}, \boldsymbol{y}) = {} & \frac{1}{2\pi} \ln |\boldsymbol{y} - \boldsymbol{x}| - \frac{1}{2\pi} \ln |\boldsymbol{y} - \bar{\boldsymbol{x}}| \\ & + \frac{s_2}{2\pi}(s_2 + is_1) \ln(\boldsymbol{v} \cdot \boldsymbol{s} - i\boldsymbol{v} \times \boldsymbol{s}) + \frac{s_2}{2\pi}(s_2 - is_1) \ln(\boldsymbol{v} \cdot \boldsymbol{s} + i\boldsymbol{v} \times \boldsymbol{s}), \end{aligned} \tag{7.51}$$

except for an additive complex constant that can be disregarded. When $s_2 = 1$, then (7.51) turns moreover into the Green's function resulting from a homogeneous Neumann boundary condition in $\mathbb{R}^2_+$ when $Z \to 0$, namely

$$G(\boldsymbol{x}, \boldsymbol{y}) = \frac{1}{2\pi} \ln |\boldsymbol{y} - \boldsymbol{x}| + \frac{1}{2\pi} \ln |\boldsymbol{y} - \bar{\boldsymbol{x}}|, \tag{7.52}$$

excepting again an additive complex constant.

At last, we observe that the expression for the Green's function (7.41) is still valid if a complex impedance $Z \in \mathbb{C}$ such that $\mathfrak{Im}\{Z\} > 0$ and $\mathfrak{Re}\{Z\} \geq 0$ is used, which is associated with dissipative wave propagation. The branch cuts of the logarithms that are contained in the exponential integral functions, though, have to be treated very carefully in this case, since they have to stay on the half-line $\Upsilon$. A straightforward evaluation of these logarithms with a complex impedance rotates the branch cuts in the $(v_1, v_2)$-plane and generates thus two discontinuous half-lines for the Green's function in the half-plane $\boldsymbol{v} \cdot \boldsymbol{s} < 0$. This undesired behavior of the branch cuts can be avoided if the complex logarithms are taken in the sense of

$$\ln\big(Z\boldsymbol{v} \cdot \boldsymbol{s} - iZ\boldsymbol{v} \times \boldsymbol{s}\big) = \ln(\boldsymbol{v} \cdot \boldsymbol{s} - i\boldsymbol{v} \times \boldsymbol{s}) + \ln(Z), \tag{7.53a}$$

$$\ln\big(Z\boldsymbol{v} \cdot \boldsymbol{s} + iZ\boldsymbol{v} \times \boldsymbol{s}\big) = \ln(\boldsymbol{v} \cdot \boldsymbol{s} + i\boldsymbol{v} \times \boldsymbol{s}) + \ln(Z), \tag{7.53b}$$

where the principal value is considered for the logarithms on the right-hand side. For the remaining terms of the Green's function, the complex impedance $Z$ can be evaluated directly without any problems.

## 7.6 Far field of the Green's function

### 7.6.1 Decomposition of the far field

The far field of the Green's function (7.41), denoted by $G^{ff}$, describes its asymptotic behavior at infinity, i.e., when $|\boldsymbol{y}| \to \infty$ and assuming that $\boldsymbol{x}$ is fixed. For this purpose, the terms of highest order at infinity are searched. Likewise as for the radiation condition, the

far field can be also decomposed into two parts, namely

$$G^{ff} = G_A^{ff} + G_S^{ff}. \tag{7.54}$$

The first part, $G_A^{ff}$, is linked with the asymptotic decaying of the fundamental solution for the Laplace equation, whereas the second part, $G_S^{ff}$, is associated with the oblique surface waves.

### 7.6.2 Asymptotic decaying

The asymptotic decaying acts above and away from the line $\boldsymbol{y}\cdot\boldsymbol{s}=0$, and is related to the logarithmic terms in (7.41), and also to the asymptotic behavior as $\boldsymbol{y}\cdot\boldsymbol{s}\to\infty$ of the exponential integral terms. In fact, due (7.39) we have for $z\in\mathbb{C}$ that

$$\mathrm{Ei}(z) \sim \frac{e^z}{z} \qquad \text{as } \ \mathfrak{Re}\{z\}\to\infty. \tag{7.55}$$

By considering the behavior (7.55) in (7.41), by remembering (7.1d), and by neglecting the exponentially decreasing terms as $\boldsymbol{y}\cdot\boldsymbol{s}\to\infty$, we obtain that

$$G(\boldsymbol{x},\boldsymbol{y}) \sim \frac{1}{2\pi}\ln|\boldsymbol{y}-\boldsymbol{x}| - \frac{1}{2\pi}\ln|\boldsymbol{y}-\bar{\boldsymbol{x}}| + \frac{s_2}{Z\pi}\,\frac{y_2+x_2}{|\boldsymbol{y}-\bar{\boldsymbol{x}}|^2}. \tag{7.56}$$

Using Taylor expansions as in Section 2.4, we have that

$$\frac{1}{2\pi}\ln|\boldsymbol{y}-\boldsymbol{x}| - \frac{1}{2\pi}\ln|\boldsymbol{y}-\bar{\boldsymbol{x}}| = -\frac{(\boldsymbol{x}-\bar{\boldsymbol{x}})\cdot\boldsymbol{y}}{2\pi|\boldsymbol{y}|^2} + \mathcal{O}\!\left(\frac{1}{|\boldsymbol{y}|^2}\right), \tag{7.57}$$

and likewise that

$$\frac{s_2}{Z\pi}\,\frac{y_2+x_2}{|\boldsymbol{y}-\bar{\boldsymbol{x}}|^2} = \frac{s_2}{Z\pi}\,\frac{y_2}{|\boldsymbol{y}|^2} + \mathcal{O}\!\left(\frac{1}{|\boldsymbol{y}|^2}\right). \tag{7.58}$$

We consider $\boldsymbol{y}=|\boldsymbol{y}|\,\hat{\boldsymbol{y}}$, being $\hat{\boldsymbol{y}}=(\cos\theta,\sin\theta)$ a unitary vector. Hence, from (7.56) and due (7.57) and (7.58), the asymptotic decaying of the Green's function is given by

$$G_A^{ff}(\boldsymbol{x},\boldsymbol{y}) = \frac{\sin\theta}{Z\pi|\boldsymbol{y}|}\big(s_2 - Zx_2\big). \tag{7.59}$$

### 7.6.3 Surface waves in the far field

The oblique surface waves present in the far field are found by studying the poles of the spectral Green's function, which determine their asymptotic behavior and which wad already done. The expression that describes them is obtained by adding (7.20) and (7.21), which implies that the Green's function behaves asymptotically, when $|\boldsymbol{y}\times\boldsymbol{s}|\to\infty$, as

$$\begin{aligned} G(\boldsymbol{x},\boldsymbol{y}) \sim\ & -i\frac{s_2}{2}(s_2+is_1)\big(1+\mathrm{sign}(\boldsymbol{v}\times\boldsymbol{s})\big)\,e^{-Z\boldsymbol{v}\cdot\boldsymbol{s}+iZ\boldsymbol{v}\times\boldsymbol{s}} \\ & -i\frac{s_2}{2}(s_2-is_1)\big(1-\mathrm{sign}(\boldsymbol{v}\times\boldsymbol{s})\big)\,e^{-Z\boldsymbol{v}\cdot\boldsymbol{s}-iZ\boldsymbol{v}\times\boldsymbol{s}}, \end{aligned} \tag{7.60}$$

or, equivalently, as

$$G(\boldsymbol{x},\boldsymbol{y}) \sim -is_2\big(s_2+is_1\,\mathrm{sign}(\boldsymbol{v}\times\boldsymbol{s})\big)\,e^{-Z\boldsymbol{v}\cdot\boldsymbol{s}+iZ|\boldsymbol{v}\times\boldsymbol{s}|}. \tag{7.61}$$

We can use again Taylor expansions to obtain the estimates

$$|\boldsymbol{v}\times\boldsymbol{s}| = |\boldsymbol{y}\times\boldsymbol{s}| - (\bar{\boldsymbol{x}}\times\boldsymbol{s})\,\mathrm{sign}(\boldsymbol{y}\times\boldsymbol{s}) + \mathcal{O}\!\left(\frac{1}{|\boldsymbol{y}\times\boldsymbol{s}|}\right), \tag{7.62}$$

$$\operatorname{sign}(\boldsymbol{v}\times\boldsymbol{s}) = \operatorname{sign}(\boldsymbol{y}\times\boldsymbol{s}) + \mathcal{O}\Big(\frac{1}{|\boldsymbol{y}\times\boldsymbol{s}|}\Big). \tag{7.63}$$

Therefore we have that

$$e^{iZ|\boldsymbol{v}\times\boldsymbol{s}|} = e^{iZ|\boldsymbol{y}\times\boldsymbol{s}|}e^{-iZ(\bar{\boldsymbol{x}}\times\boldsymbol{s})\operatorname{sign}(\boldsymbol{y}\times\boldsymbol{s})}\left(1+\mathcal{O}\Big(\frac{1}{|\boldsymbol{y}\times\boldsymbol{s}|}\Big)\right). \tag{7.64}$$

The surface-wave behavior, due (7.61), (7.63), and (7.64), is thus given by

$$G_S^{ff}(\boldsymbol{x},\boldsymbol{y}) = -is_2\big(s_2+is_1\operatorname{sign}(\boldsymbol{y}\times\boldsymbol{s})\big)\,e^{-Z\boldsymbol{y}\cdot\boldsymbol{s}+iZ|\boldsymbol{y}\times\boldsymbol{s}|}e^{Z\bar{\boldsymbol{x}}\cdot\boldsymbol{s}-iZ(\bar{\boldsymbol{x}}\times\boldsymbol{s})\operatorname{sign}(\boldsymbol{y}\times\boldsymbol{s})}. \tag{7.65}$$

### 7.6.4 Complete far field of the Green's function

On the whole, the asymptotic behavior of the Green's function as $|\boldsymbol{y}|\to\infty$ can be characterized through the addition of (7.56) and (7.61), namely

$$\begin{aligned} G(\boldsymbol{x},\boldsymbol{y}) \sim{}& \frac{1}{2\pi}\ln|\boldsymbol{y}-\boldsymbol{x}| - \frac{1}{2\pi}\ln|\boldsymbol{y}-\bar{\boldsymbol{x}}| + \frac{s_2}{Z\pi}\,\frac{y_2+x_2}{|\boldsymbol{y}-\bar{\boldsymbol{x}}|^2} \\ &- is_2\big(s_2+is_1\operatorname{sign}(\boldsymbol{v}\times\boldsymbol{s})\big)\,e^{-Z\boldsymbol{v}\cdot\boldsymbol{s}+iZ|\boldsymbol{v}\times\boldsymbol{s}|}. \end{aligned} \tag{7.66}$$

Consequently, the complete far field of the Green's function, due (7.54), is given by the addition of (7.59) and (7.65), i.e., by

$$\begin{aligned} G^{ff}(\boldsymbol{x},\boldsymbol{y}) = {}& \frac{\sin\theta}{Z\pi|\boldsymbol{y}|}\big(s_2-Zx_2\big) \\ &- is_2\big(s_2+is_1\operatorname{sign}(\boldsymbol{y}\times\boldsymbol{s})\big)\,e^{-Z\boldsymbol{y}\cdot\boldsymbol{s}+iZ|\boldsymbol{y}\times\boldsymbol{s}|}e^{Z\bar{\boldsymbol{x}}\cdot\boldsymbol{s}-iZ(\bar{\boldsymbol{x}}\times\boldsymbol{s})\operatorname{sign}(\boldsymbol{y}\times\boldsymbol{s})}. \end{aligned} \tag{7.67}$$

It is this far field (7.67) that justifies the radiation condition (7.1*e–f*). When the first term in (7.67) dominates, i.e., the asymptotic decaying (7.59), then it is the behavior (7.1e) that matters. Conversely, when the second term in (7.67) dominates, i.e., the oblique surface waves (7.65), then (7.1f) is the one that holds. The interface between both asymptotic behaviors can be determined by equating the amplitudes of the two terms in (7.67), i.e., by searching values of $\boldsymbol{y}$ at infinity such that

$$\frac{s_2}{Z\pi|\boldsymbol{y}|} = s_2\,e^{-Z\boldsymbol{y}\cdot\boldsymbol{s}}, \tag{7.68}$$

where the values of $\boldsymbol{x}$ can be neglected, since they remain relatively near the origin. By taking the logarithm in (7.68) and perturbing somewhat the result so as to avoid a singular behavior at the origin, we obtain finally that this interface is described by

$$\boldsymbol{y}\cdot\boldsymbol{s} = \frac{1}{Z}\ln\big(1+Z\pi|\boldsymbol{y}|\big). \tag{7.69}$$

We remark that the asymptotic behavior (7.66) of the Green's function and the expression (7.67) of its complete far field do no longer hold if a complex impedance $Z$ such that $\mathfrak{Im}\{Z\}>0$ and $\mathfrak{Re}\{Z\}\geq 0$ is used, specifically the parts (7.61) and (7.65) linked

with the oblique surface waves. A careful inspection shows that in this case the surface-wave behavior, as $|\boldsymbol{y}\times\boldsymbol{s}|\to\infty$, decreases exponentially and is given by

$$G(\boldsymbol{x},\boldsymbol{y})\sim\begin{cases}-is_2\big(s_2+is_1\,\mathrm{sign}(\boldsymbol{v}\times\boldsymbol{s})\big)\,e^{-|Z|\boldsymbol{v}\cdot\boldsymbol{s}+iZ|\boldsymbol{v}\times\boldsymbol{s}|} & \text{if } \boldsymbol{v}\cdot\boldsymbol{s}>0,\\ -is_2\big(s_2+is_1\,\mathrm{sign}(\boldsymbol{v}\times\boldsymbol{s})\big)\,e^{-Z\boldsymbol{v}\cdot\boldsymbol{s}+iZ|\boldsymbol{v}\times\boldsymbol{s}|} & \text{if } \boldsymbol{v}\cdot\boldsymbol{s}\le 0.\end{cases}\tag{7.70}$$

Therefore the surface-wave part of the far field is now expressed, if $\boldsymbol{y}\cdot\boldsymbol{s}>0$, as

$$G_S^{ff}(\boldsymbol{x},\boldsymbol{y})=-is_2\big(s_2+is_1\,\mathrm{sign}(\boldsymbol{y}\times\boldsymbol{s})\big)\,e^{-|Z|\boldsymbol{y}\cdot\boldsymbol{s}+iZ|\boldsymbol{y}\times\boldsymbol{s}|}e^{|Z|\bar{\boldsymbol{x}}\cdot\boldsymbol{s}-iZ(\bar{\boldsymbol{x}}\times\boldsymbol{s})\,\mathrm{sign}(\boldsymbol{y}\times\boldsymbol{s})},\tag{7.71}$$

and if $\boldsymbol{y}\cdot\boldsymbol{s}\le 0$, then it becomes

$$G_S^{ff}(\boldsymbol{x},\boldsymbol{y})=-is_2\big(s_2+is_1\,\mathrm{sign}(\boldsymbol{y}\times\boldsymbol{s})\big)\,e^{-Z\boldsymbol{y}\cdot\boldsymbol{s}+iZ|\boldsymbol{y}\times\boldsymbol{s}|}e^{Z\bar{\boldsymbol{x}}\cdot\boldsymbol{s}-iZ(\bar{\boldsymbol{x}}\times\boldsymbol{s})\,\mathrm{sign}(\boldsymbol{y}\times\boldsymbol{s})}.\tag{7.72}$$

The asymptotic decaying (7.56) and its far-field expression (7.59), on the other hand, remain the same when a complex impedance is used.